An Update on Mineral Inclusions and Their Composition in Ruby from the Bo Rai Gem Field in Trat Province, Eastern Thailand

Supparat Promwongnan and Chakkaphan Sutthirat

ABSTRACT: The Bo Rai alluvial gem field in Trat Province, eastern Thailand, was a major mining site for Thai ruby during the early 1980s, and this material continues to circulate in the gem market worldwide. For this study, approximately 1,000 Bo Rai ruby samples were examined and pre-screened for mineral inclusions. The rough stones usually formed platy, waterworn, tabular crystals with etched or resorbed surfaces. UV-Vis-NIR spectroscopy indicated a relatively high Fe content, which was confirmed by trace-element analysis. Solid inclusions typically consisted of Al-rich pyroxene, plagioclase and pyrope with subordinate sillimanite and spinel (both of which are reported here for the first time), as well as sulphides and silicate melt inclusions. The inclusion assemblage of pyroxene, plagioclase, pyrope and spinel closely resembles the mineralogy of mafic granulite xenoliths in alkali basalt associated with the Bo Rai gem field, which supports ruby formation in mafic granulite prior to being transported to the earth's surface via basaltic eruptions.

The Journal of Gemmology, **36**(7), 2019, pp. 634–645, http://doi.org/10.15506/JoG.2019.36.7.634

For decades, Thai ruby has been well known for its attractive purplish red colour, which can be heat treated to deep red (Figure 1). The stones typically occur in alluvial deposits associated with Cenozoic intraplate basalts (Vichit 1992; Sutthirat *et al.* 1994). During the early 1980s (Keller 1982), the Bo Rai gem field—located in Trat Province, eastern Thailand, close to Cambodia—was the main source of Thai ruby, and associated minerals in the alluvium include garnet, magnetite, pyroxene and ilmenite (Vichit *et al.* 1978; Vichit 1992). Some other significant mining areas for Thai rubies include Na Wong and Nong Bon in Trat Province and Pong Nam Ron and Bo Welu in Chanthaburi Province. In addition, minor Thai ruby occurrences are known in Ubon Ratchathani and Si Sa Ket Provinces in the north-eastern part of the country (Vichit 1992; Pattamalai 2015). Although there is currently very little production of Thai ruby, the material continues to circulate in the global gem market.

Several authors have previously described the properties of Thai ruby (e.g. Gübelin 1971; Intasopa *et al.* 1999; Saminpanya *et al.* 2003; Saminpanya & Sutherland 2011; Sangsawong *et al.* 2017). Moreover, various types of mineral inclusions in Thai corundum (both ruby and sapphire) have been investigated (Gübelin 1940). Optical microscopy, Raman spectroscopy and powder X-ray diffraction have been used to identify the mineral inclusions in Thai corundum (e.g. Gübelin & Koivula 1986; Koivula & Fryer 1987; Intasopa *et al.* 1999; Hughes 2017; Saeseaw *et al.* 2017; Sangsawong *et al.* 2017), whereas the chemical composition of these minerals has been investigated using electron probe

Figure 1: This collection shows the deep red appearance of high-quality Thai rubies (here, 0.87–2.86 ct). They have been heat treated to improve their colour. Stones courtesy of Thai Lapidary International Co. Ltd; photo by S. Promwongnan.

micro-analysis (EPMA; e.g. Gübelin 1971; Guo *et al.* 1994; Sutherland *et al.* 1998a; Sutthirat *et al.* 2001; Khamloet *et al.* 2014), proton microprobe analysis (Guo *et al.* 1994) and scanning electron microscopy with energy-dispersive X-ray spectroscopy (Saminpanya & Sutherland 2011).

Sutherland *et al.* (1998b) separated the mineral inclusions in basaltic-type gem corundum into two groups: metamorphic origin (e.g. Mg-rich spinel, sapphirine, 'fassaite' [pyroxene with a low Fe content] and garnet) and magmatic origin (e.g. plagioclase, zircon, Fe-Ti oxides, Nb-Ta oxides, U-Th oxides and rare-earth phosphates). Typical inclusions in Thai rubies have been reported by various researchers as pyrrhotite, apatite, garnet, diopside, sapphirine and plagioclase (Gübelin 1971; Intasopa *et al.* 1999; Sutthirat *et al.* 2001; Saminpanya & Sutherland 2011), and some of these authors also suggested that Thai ruby possibly crystallised from high-grade metamorphosed mafic rocks. Recently, Sutthirat *et al.* (2018) documented ruby-bearing mafic granulite xenoliths from the Bo Rai deposit, which provide the most significant direct evidence for the primary metamorphic formation of Thai ruby.

In this study, approximately 1,000 unheated Bo Rai rubies were pre-screened to select samples for examination of mineral inclusions. (These included some purple sapphires, although the sample collection is here classified as 'ruby' since during heat treatment the purple stones are usually transformed into the colour range of ruby.) Our examination of the inclusions particularly focused on mineral chemistry, which is the primary aim of this project. In addition, the samples' gemmological properties, optical and spectroscopic characteristics and trace-element compositions were investigated.

MATERIALS AND METHODS

Using a gemmological microscope, we selected 88 samples (containing 141 mineral inclusions) for examination from the approximately 1,000 unheated rough Bo Rai rubies. The samples were carefully cut and polished with a Facetron faceting machine to expose their mineral inclusions at the surface for analysis. After polishing, they ranged from 0.006 to 0.17 g.

Standard gemmological properties (i.e. colour, diaphaneity, RIs and fluorescence reactions to long- and short-wave UV radiation) were recorded for all 88 samples. (Specific gravity was not measured due to their small size.) Internal and external features were observed with a gemmological microscope, and an attached Canon EOS 7D camera was used for photomicrography.

Mid-infrared spectra (4000–400 cm^{-1}) were obtained in transmittance mode for all 88 samples (resolution of 4.0 cm^{-1} and 128 scans) using a Thermo-Nicolet 6700 Fourier-transform infrared (FTIR) spectrometer. Ultraviolet-visible-near infrared (UV-Vis-NIR) absorption spectra were obtained for all samples using a PerkinElmer Lambda 950 spectrophotometer in the range 250–800 nm with a 3.0 nm sampling interval and 441 nm/minute scan speed. Good-quality trace-element analyses were obtained for 78 of the samples by energy-dispersive X-ray fluorescence (EDXRF) spectroscopy with an Eagle III system; semi-quantitative results for Al, Cr, Fe, Ti, V and Ga were subsequently normalised and reported as oxides. Preliminary identification of the mineral inclusions in all samples was performed with a Renishaw inVia Raman microspectroscopy system utilising 532 nm excitation from an Nd:YAG laser. The magnification of the objective lens was 50×. All of the analyses mentioned above were done at the Gem Testing Laboratory of the Gem and Jewelry Institute of Thailand (Public Organization) in Bangkok.

Mineral inclusions in 41 of the rubies were selected for major- and minor-element analysis by EPMA. The samples were mounted in epoxy resin and polished prior to carbon coating and analysis with a JEOL JXA-8100 instrument based at the Geology Department, Faculty of Science, Chulalongkorn University, Bangkok. Operating conditions included an accelerating voltage of 15.0 kV and a sample current of ~25.0 nA, with a focused beam of <1 µm in diameter. Measurement times for each element were set at 30 seconds for peak counts and 10 seconds for background counts. The analytical results were then subjected to automated ZAF correction and reported as weight percent oxides. The ferrous and ferric iron contents of some minerals (e.g. pyroxene, garnet and spinel) were calculated using the methodology of Droop (1987).

RESULTS

Gemmological Properties

The samples typically formed platy waterworn crystals that were semi-transparent to transparent. Their colouration (see, e.g., Figure 2) can be summarised as follows: moderate to slightly purplish red (pR, ~2% of the collection), purple-red to red-purple (PR-RP, ~79%), reddish purple (rP, ~17%) and purple (P, ~2%). They had RIs of 1.760–1.771 and birefringence values of 0.008–0.010. They showed inert-to-moderate red fluorescence to long-wave UV radiation and were inert to short-wave UV.

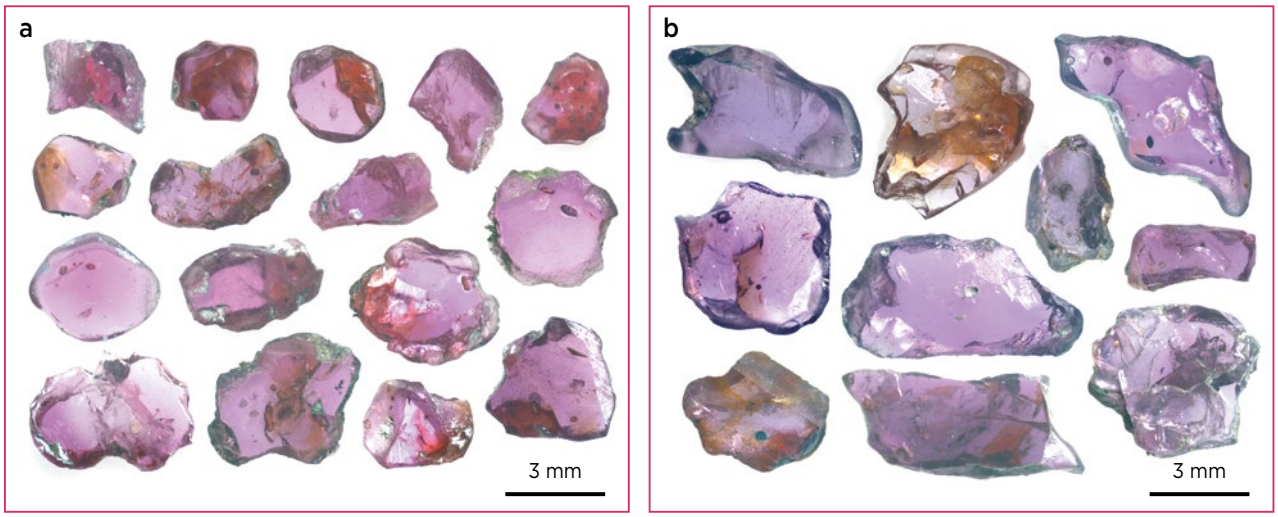

Figure 2: Representative rough pieces of Bo Rai gem corundum show a range of colour: (**a**) moderate to slightly purplish red to red-purple, and (**b**) reddish purple to purple. Most of the samples have been polished on both sides to expose mineral inclusions on their surfaces. Photos by S. Promwongnan.

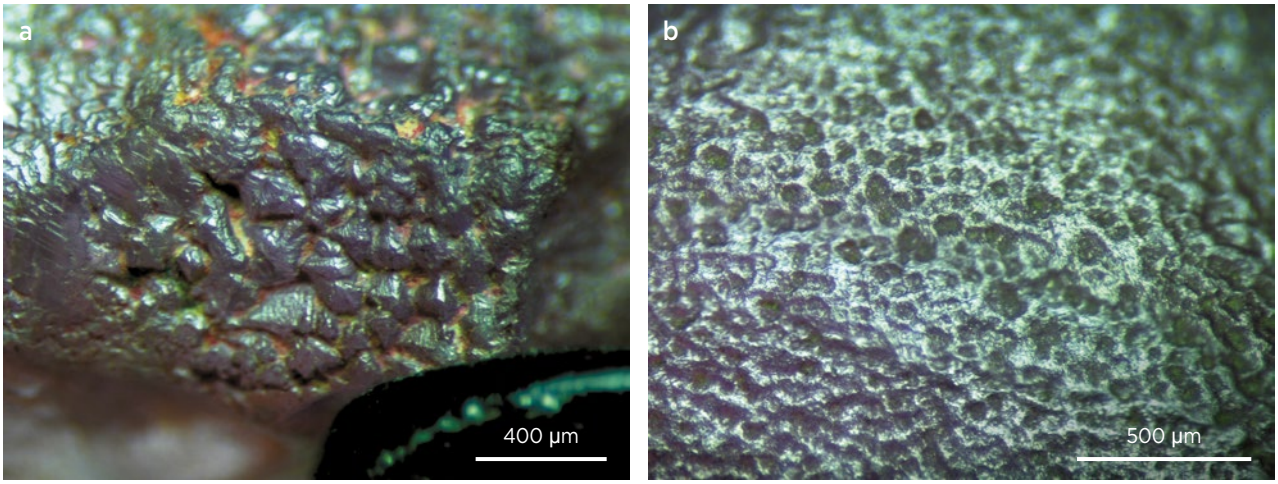

Figure 3: These photomicrographs show etched and dissolved features on the surfaces of two rough rubies from Bo Rai. Photomicrographs by S. Promwongnan in reflected light.

Before being polished into plates for inclusion examination, some of the samples presented etched or dissolved surfaces (Figure 3).

Spectroscopic Features

The FTIR spectra of the rubies showed similar patterns for all the samples, including bands at approximately 2363 and 2342 cm^{-1} due to CO_2, and at 2924 and 2852 cm^{-1} due to C-H stretching (Figure 4; cf. Beran & Rossman 2006). Some samples (e.g. Figure 4, red spectrum) also presented a shoulder at about 3170 cm^{-1} and a series of sharp bands at 3697, 3669, 3652 and 3620 cm^{-1} that relate to the hydrous component of a kaolinite-group mineral (cf. Beran & Rossman 2006; Schwarz *et al.* 2008).

UV-Vis-NIR spectra showed an absorption at ~330 nm related to high Fe content (Figure 5, blue spectrum), and in some samples this absorption was so strong that the spectra presented a cut-off in this region (Figure 5, red spectrum). Most of the pR and PR-RP samples showed distinct Cr-related absorption features at around 410, 560 and 694 nm (Figure 5, blue spectrum), consistent with their dominantly red colour. However, those samples falling in the rP to P colour range clearly showed intense Fe-related absorptions at 387 and 450 nm (Figure 5, red spectrum).

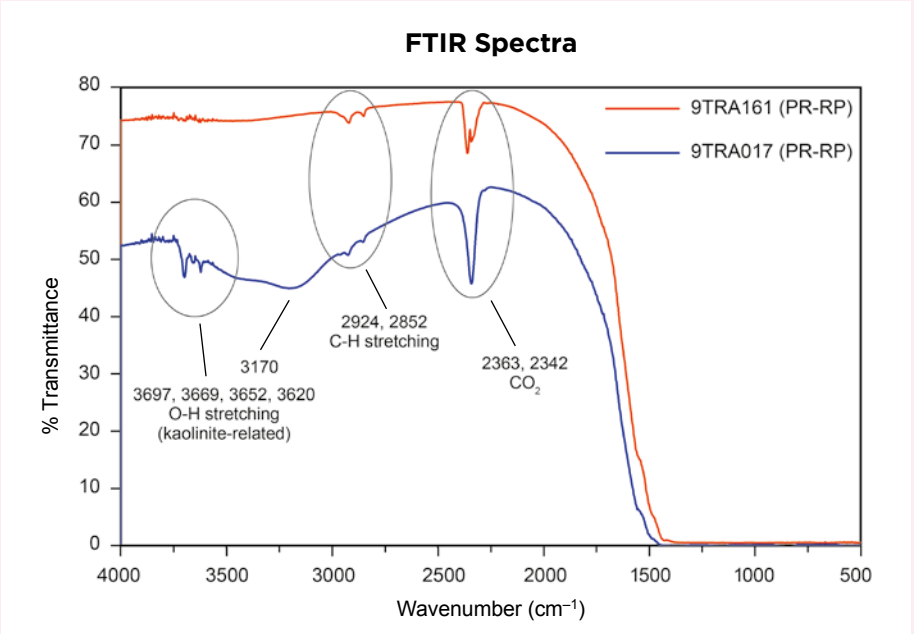

Figure 4: Representative mid-IR spectra of two purple-red to red-purple ruby samples from Bo Rai reveal bands at approximately 2363 and 2342 cm^{-1} due to CO_2, and at 2924 and 2852 cm^{-1} due to C-H stretching. Sharp features at 3697, 3669, 3652 and 3620 cm^{-1} in the lower spectrum are due to O-H stretching related to a kaolinite phase.

EDXRF Analyses

Semi-quantitative chemical analyses of the Bo Rai samples varied within fairly narrow ranges (e.g. Table I). Overall, Fe and Ti concentrations ranged from ~0.35 to 1.26 wt.% Fe_2O_3 and 0.01 to 0.67 wt.% TiO_2, respectively. Chromium contents fell within the range of 0.06–0.92 wt.% Cr_2O_3. Overall, the rP to P samples contained less Cr than those falling into the pR to PR-RP colour range. About 20% of the samples yielded V contents below the detection limit, and the highest value was only ~0.04 wt.% V_2O_5. Gallium was below the detection limit in some samples, while the greatest amount measured was ~0.03 wt.% Ga_2O_3.

Internal Features

Apart from the mineral inclusions described below, a variety of internal features could be seen in our samples with the microscope. The most typical characteristics were minute crystals (too small to be reliably identified by Raman or microprobe analysis) surrounded by equatorial thin films (Figure 6a). Also present were parallel twin planes, needle-like inclusions (Figure 6b) and partially healed fractures ('fingerprints'). In addition, some samples hosted inclusions containing multiple fluid/gas phases (Figure 7a) or two-phase assemblages consisting of a solidified silicate melt and a gas phase (possibly CO_2; Figure 7b). The latter

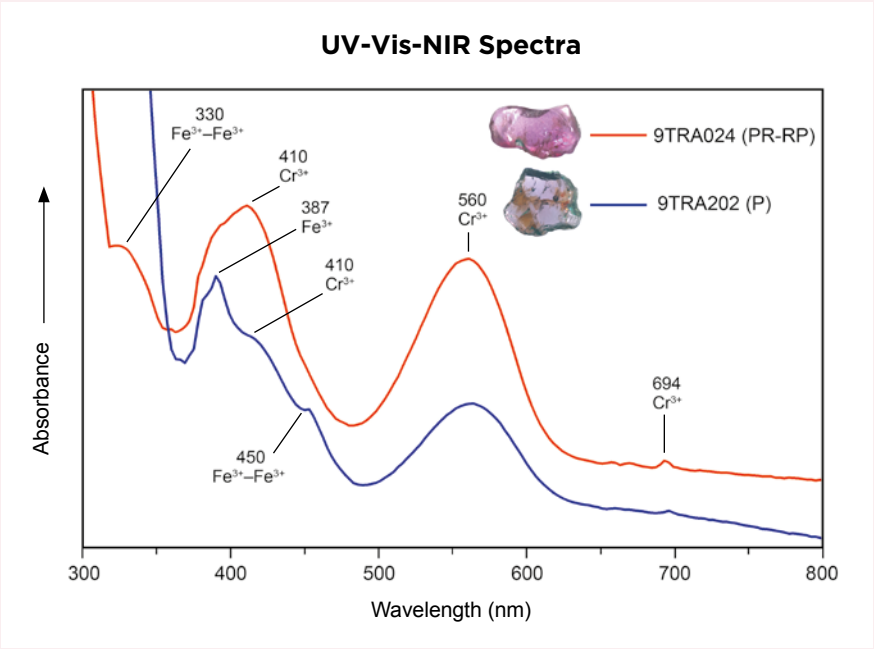

Figure 5: These representative UV-Vis-NIR absorption spectra of Bo Rai gem corundum (taken of the ordinary ray) display features due to Cr and Fe. A red-purple ruby sample reveals an Fe^{3+}-related absorption feature at ~330 nm and Cr^{3+}-dominated peaks at 410, 560 and 694 nm causing the red colour. A purple sample reveals obvious Fe^{3+}-related peaks with a cut-off at ~330 nm and a peak at 387 nm. The path lengths of the beam through the samples were 0.74 mm (9TRA024) and 1.20 mm (9TRA202).

Table I: Representative semi-quantitative EDXRF analyses of the Bo Rai ruby sample set.

Colour range	Purple-red to red-purple						Reddish purple to purple						
Sample no.	9TRA 075	9TRA 045	9TRA 208	9TRA 212	9TRA 124	9TRA 078	9TRA 219	9TRA 217	9TRA 137	9TRA 156	9TRA 228	9TRA 029	9TRA 155
Oxide (wt.%)													
V_2O_5	0.01	nd*	0.01	0.01	0.01	nd	0.01	nd	0.04	0.01	0.01	nd	0.01
TiO_2	0.44	0.17	0.04	0.06	0.08	0.67	0.04	0.05	0.07	0.08	0.02	0.02	0.08
Al_2O_3	98.16	98.49	99.13	99.09	98.75	97.83	99.07	98.91	98.54	98.95	99.29	99.44	98.83
Cr_2O_3	0.50	0.48	0.27	0.26	0.35	0.45	0.24	0.26	0.31	0.18	0.08	0.06	0.12
Ga_2O_3	nd	0.02	0.01	0.01	0.02	nd	nd	0.01	0.02	nd	0.01	0.01	0.01
Fe_2O_3	0.89	0.84	0.55	0.57	0.79	1.05	0.64	0.77	1.03	0.78	0.60	0.46	0.95
Total	100.00	100.00	100.00	100.00	100.00	100.00	100.00	100.00	100.00	100.00	100.00	100.00	100.00

*Abbreviation: nd = not detected.

commonly formed rounded shapes, and EPMA analyses of the melt inclusions showed major Si, Al and Ca, with minor Fe, Mg, Na and K.

Pyroxene was the most common mineral inclusion identified in this study, with 122 of these crystals observed in 71 of the 88 samples of Bo Rai ruby. It usually formed rounded crystals with ellipsoidal or columnar shapes (Figure 8). Most were colourless, but some appeared light brown (Figure 8c). Their chemical composition characterised them as Al-rich pyroxene, close to diopside composition (see Table II and Figure 9; cf. Clark & Papike 1968).

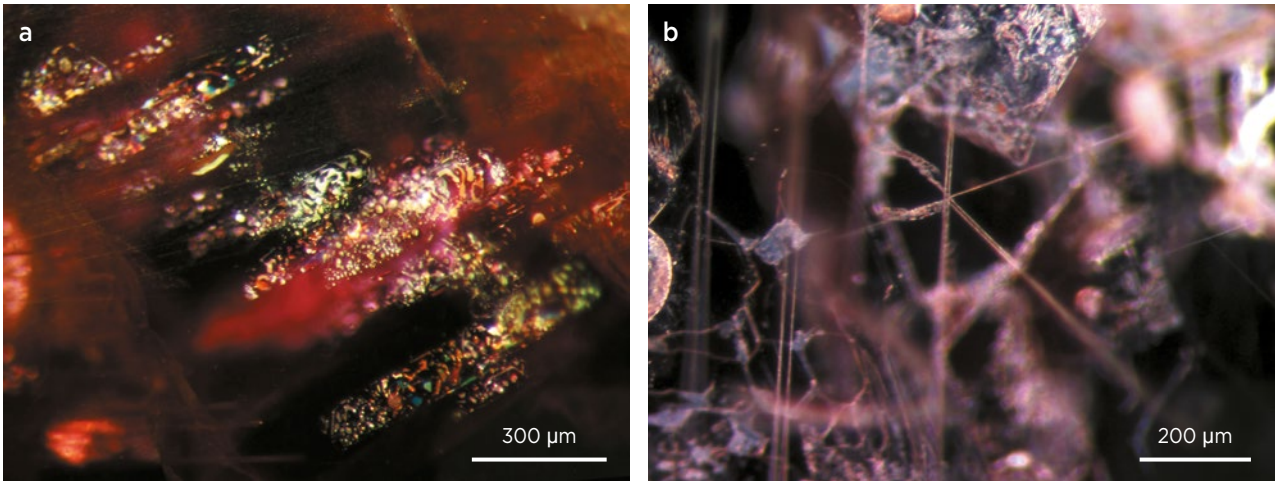

Figure 6: Internal features observed in the Bo Rai ruby samples include: (**a**) equatorial thin films surrounding minute crystals and (**b**) needle-like inclusions. Photomicrographs by S. Promwongnan; darkfield illumination with fibre-optic light.

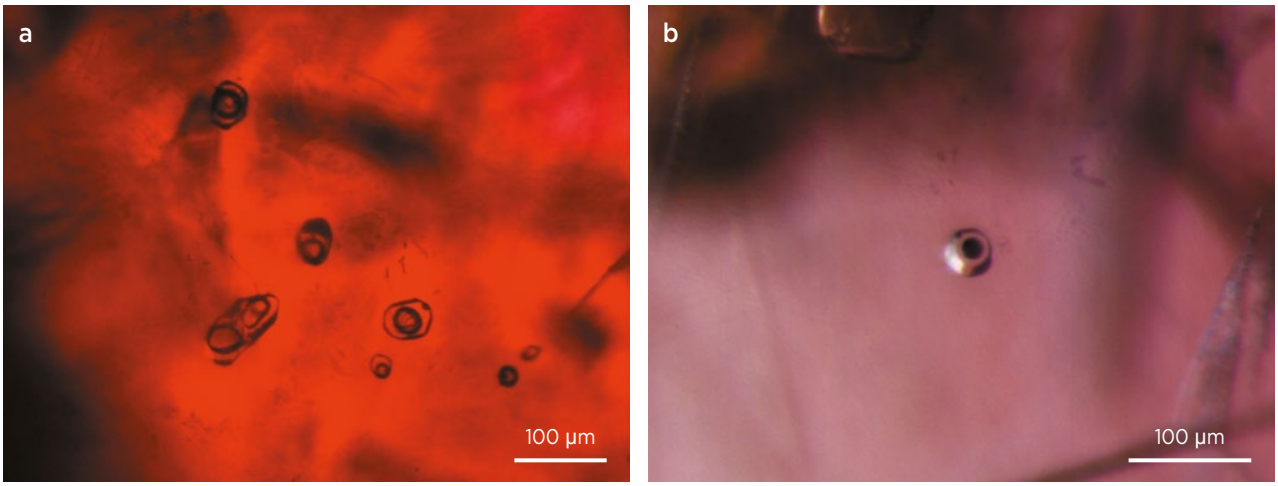

Figure 7: (**a**) These inclusions in a Bo Rai ruby appear to contain multiple fluid/gas phases. (**b**) Silicate melt inclusions in the rubies were associated with a gas phase (likely CO_2). Photomicrographs by S. Promwongnan; (a) darkfield illumination and (b) brightfield illumination with fibre-optic light.

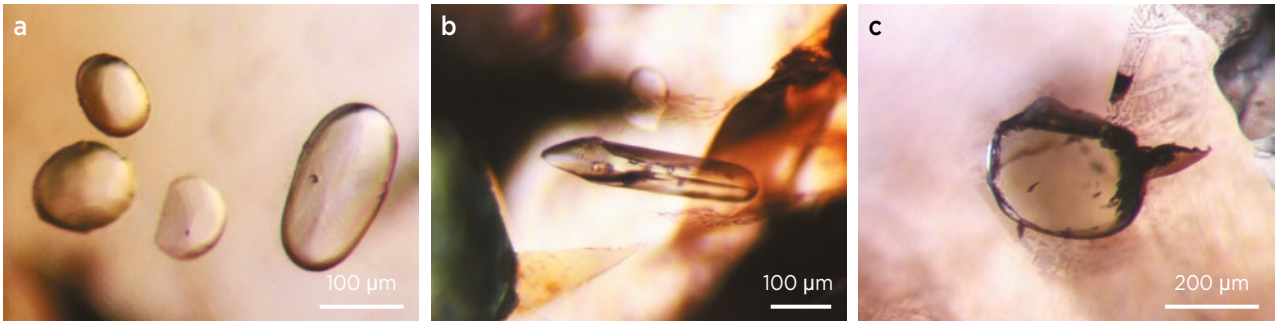

Figure 8: Pyroxene is a common mineral inclusion in Bo Rai ruby and typically forms (**a**) ellipsoidal or (**b**) columnar shapes. Most are colourless, but some are light brown (**c**). Photomicrographs by S. Promwongnan; brightfield illumination with fibre-optic light.

Table II: Representative EPMA analyses of pyroxene inclusions in the Bo Rai ruby sample set.

Sample no.	9TRA 016-1	9TRA 023-1	9TRA 118-2	9TRA 124-1	9TRA 036-1	9TRA 156-1
Oxide (wt.%)						
SiO_2	46.51	47.10	46.85	46.16	46.55	47.56
TiO_2	0.14	0.04	0.03	0.08	0.11	0.60
Al_2O_3	14.68	14.69	14.50	15.81	13.88	14.15
Cr_2O_3	0.14	0.08	0.04	0.13	0.04	0.07
FeO_{tot}	2.25	2.25	3.39	2.79	2.67	3.51
MnO	nd*	0.04	0.08	0.02	0.01	0.05
MgO	11.93	11.65	11.97	11.10	13.32	11.01
CaO	22.09	21.76	20.98	22.24	21.34	21.47
Na_2O	1.02	1.20	1.44	0.87	0.97	1.41
K_2O	0.01	0.01	0.01	0.02	0.01	nd
Total	98.76	98.81	99.29	99.21	98.89	99.81
Formula per 6(O)						
Si	1.705	1.722	1.713	1.687	1.706	1.731
Ti	0.004	0.001	0.001	0.002	0.003	0.016
Al	0.634	0.633	0.625	0.681	0.599	0.607
Cr	0.004	0.002	0.001	0.004	0.001	0.002
Fe^{3+}	0.025	0.005	0.071	0.000	0.077	0.000
Fe^{2+}	0.044	0.063	0.032	0.085	0.005	0.107
Mn	nd	0.001	0.002	0.001	0.000	0.002
Mg	0.652	0.635	0.653	0.605	0.727	0.597
Ca	0.868	0.853	0.822	0.871	0.838	0.837
Na	0.073	0.085	0.102	0.062	0.069	0.099
K	0.000	0.001	0.000	0.001	0.001	nd
Total	4.008	4.002	4.024	3.999	4.026	3.998
% Ca	55.50	55.00	54.55	55.80	53.38	54.32
% Mg	41.69	40.94	43.33	38.76	46.31	38.74
% Fe	2.81	4.06	2.12	5.45	0.32	6.94
Total	100.00	100.00	100.00	100.00	100.00	100.00

*Abbreviation: nd = not detected.

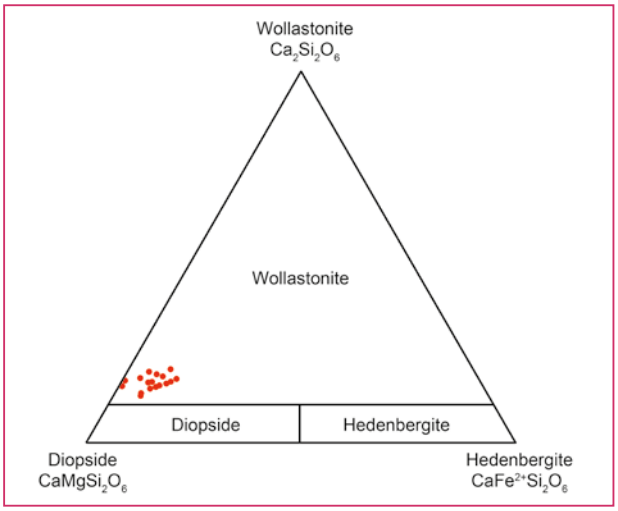

Figure 9: A compositional plot of Al-rich pyroxene inclusions analysed in the Bo Rai rubies shows them to be close to diopside composition. The apparent shift from diopside is caused by substitution from the Ca-Tschermak's component ($CaAl_2SiO_6$), which is not taken into account by this diagram. (diagram after Morimoto *et al.* 1988).

Garnet commonly formed subhedral crystals that appeared either colourless or pale purplish red (Figure 10a). The garnet inclusion in one sample (9TRA053) was oriented along the trigonal structure of the host ruby (Figure 10b). The dominant composition of the garnet inclusions was pyrope, and most had very low Cr contents (see Table III). This is similar to the composition of garnet inclusions reported previously in Thai ruby (Sutthirat *et al.* 2001; Saminpanya & Sutherland 2011). One elongated garnet inclusion associated with black crystals (probably a sulphide; Figure 10c) in sample 9TRA029 contained higher Fe and slightly lower Mg than most of the garnets analysed in our samples.

Feldspar inclusions were observed in four of the samples. They usually formed rounded to ellipsoidal grains (Figure 11) with chemical compositions that indicate plagioclase (i.e. bytownite: $Ab_{11-15}An_{85-89}Or_{0.1-0.2}$). One

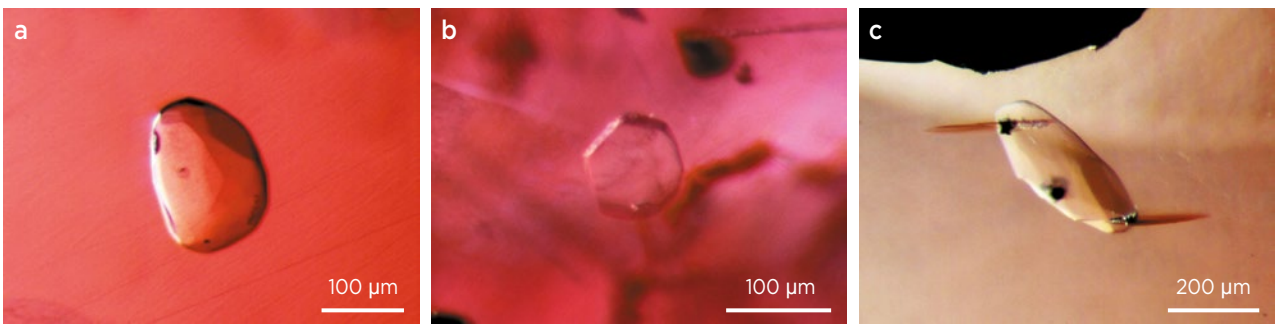

Figure 10: Garnet inclusions in Bo Rai ruby consist of low-Cr pyrope that usually form (**a**) colourless to pale purplish red crystals. (**b**) In one sample, a garnet inclusion clearly reflects the trigonal structure of the host ruby. (**c**) Another ruby sample hosts a garnet inclusion that was shown to contain relatively higher Fe and lower Mg, together with minute black crystals (likely a sulphide). Photomicrographs by S. Promwongnan; brightfield illumination with fibre-optic light.

Table III: Representative EPMA analyses of garnet, sillimanite and spinel inclusions in the Bo Rai ruby sample set.

Mineral	Garnet (pyrope)							Sillimanite		Spinel
Sample no.	9TRA 049-1	9TRA 053-1	9TRA 053-2	9TRA 206-3	9TRA 215-1	9TRA 218-1	9TRA 029-1	9TRA 169-1	9TRA 024-1	9TRA 024-2
Oxide (wt.%)										
SiO_2	41.77	42.56	41.94	41.88	42.07	41.43	41.45	36.60	36.49	0.09
TiO_2	0.02	0.01	0.03	0.01	0.05	0.02	0.05	nd*	nd	nd
Al_2O_3	23.01	23.30	23.32	22.65	23.39	24.12	23.09	62.42	62.24	67.59
Cr_2O_3	0.18	0.06	0.10	0.05	0.09	0.10	0.02	0.02	0.21	1.41
FeO_{tot}	6.55	7.09	7.05	7.21	9.27	6.29	11.29	0.39	0.73	8.12
MnO	0.20	0.22	0.16	0.20	0.19	0.12	0.23	nd	0.01	0.03
MgO	18.33	17.97	18.27	17.21	15.69	18.71	15.65	0.07	0.12	22.59
CaO	8.78	8.48	8.35	9.43	9.33	9.90	8.58	0.27	0.16	nd
K_2O	nd	nd	nd	nd	nd	nd	0.01	0.18	0.08	0.01
Na_2O	0.02	0.02	0.02	nd	nd	nd	nd	0.03	0.03	0.01
Total	98.85	99.70	99.73	100.69	100.07	99.73	100.36	99.98	100.07	99.85
Formula	per 12(O)							per 20(O)		per 4(O)
Si	3.004	3.033	3.005	3.030	3.023	2.933	2.997	3.969	3.960	0.002
Ti	0.001	0.001	0.002	0.001	0.003	0.001	0.003	nd	nd	nd
Al	1.950	1.957	1.969	1.932	1.981	2.012	1.967	7.977	7.960	1.969
Cr	0.010	0.004	0.006	0.003	0.005	0.006	0.001	0.002	0.018	0.028
Fe^{3+}	0.048	0.000	0.023	0.005	0.000	0.169	0.051	0.035	0.066	0.000
Fe^{2+}	0.346	0.422	0.399	0.432	0.557	0.203	0.631	—	—	0.168
Mn	0.012	0.013	0.010	0.012	0.012	0.007	0.014	nd	0.001	0.001
Mg	1.965	1.908	1.951	1.856	1.681	1.974	1.687	0.011	0.019	0.832
Ca	0.677	0.647	0.641	0.731	0.718	0.751	0.665	0.031	0.019	nd
K	nd	nd	nd	nd	nd	nd	0.001	0.025	0.011	0.000
Na	0.003	0.002	0.003	nd	nd	nd	nd	0.006	0.006	0.000
Total	8.016	7.987	8.008	8.002	7.981	8.057	8.017	12.05	12.060	3.000

*Abbreviation: nd = not detected.

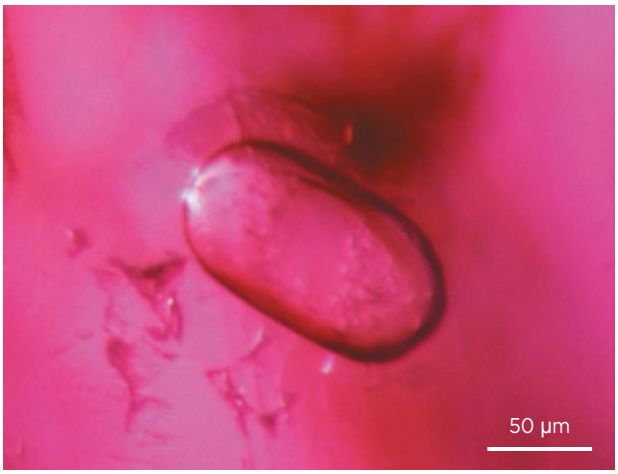

Figure 11: Plagioclase forms rounded to ellipsoidal grains in Bo Rai ruby. Photomicrograph by S. Promwongnan; brightfield illumination with fibre-optic light.

inclusion of andesine ($Ab_{56}An_{38}Or_6$) was also found in sample 9TRA031 (see Table IV and Figure 12).

Sillimanite was hosted by a fluid inclusion in sample 9TRA169 (Figure 13a). Moreover, a composite sillimanite-spinel inclusion was observed in sample 9TRA024 (Figure 13b), and it could be clearly differentiated using backscattered-electron imaging (Figure 13c). This is the first report of both sillimanite and spinel inclusions in Thai ruby. The sillimanite contained traces of Fe and Mg, and the spinel also contained some Fe: $(Mg_{0.83}Fe_{0.17})Al_2O_4$ (again, see Table III).

Sulphide inclusions formed metallic opaque black crystals with rounded or sub-hexagonal shapes (Figure 14). They were mostly present as tiny rounded grains that were each surrounded by a tension disc. EPMA analyses of the sulphides usually showed low total compositions,

Table IV: Representative EPMA analyses of plagioclase inclusions in the Bo Rai ruby sample set.

Sample no.	9TRA017-1	9TRA031-1	9TRA171-8	9TRA219-2
Mineral	**Bytownite**	**Andesine**	**Bytownite**	**Bytownite**
Oxide (wt.%)				
SiO_2	47.20	58.17	45.34	46.31
TiO_2	nd*	0.08	0.01	nd
Al_2O_3	33.36	24.72	33.87	34.47
CaO	17.52	7.52	18.13	17.02
FeO	0.13	0.46	0.42	0.22
MnO	nd	0.02	0.03	nd
MgO	0.01	0.64	nd	0.07
K_2O	0.02	1.05	0.02	0.03
Na_2O	1.68	6.02	1.48	1.14
Total	99.92	98.68	99.30	99.26
Formula per 8(O)				
Si	2.171	2.643	2.111	2.139
Ti	nd	0.003	0.000	nd
Al	1.808	1.324	1.858	1.876
Ca	0.863	0.366	0.905	0.842
Fe	0.005	0.017	0.016	0.008
Mn	nd	0.001	0.001	nd
Mg	0.001	0.043	nd	0.005
K	0.001	0.061	0.001	0.002
Na	0.149	0.530	0.134	0.102
Total	4.998	4.988	5.026	4.974
Element (at.%)				
Ca	85.15	38.27	87.02	89.02
Na	14.73	55.40	12.87	10.79
K	0.12	6.34	0.11	0.19

*Abbreviation: nd = not detected.

and apart from Fe and S, Ni and Cu were present as major and minor components in some samples (Table V). The sulphide inclusion in ruby sample 9TRA231 yielded the composition of pyrrhotite (Fe_7S_8). Others were closer to compositions of pentlandite ($[Fe,Ni]_9S_8$; sample 9TRA055) or digenite (Cu_9S_5; sample 9TRA160).

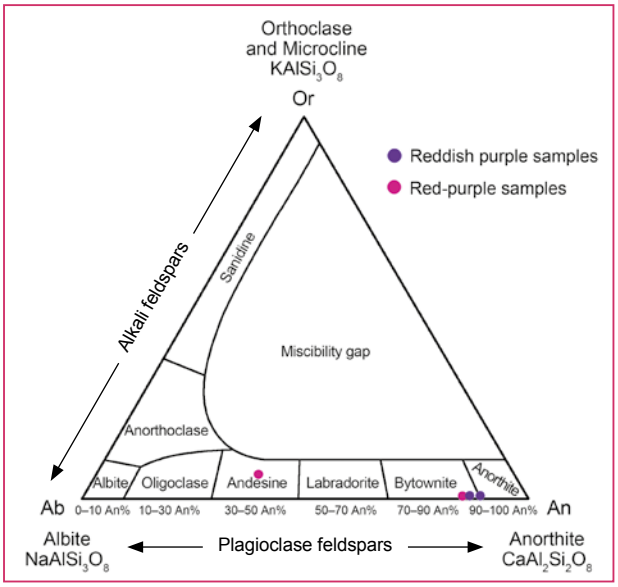

Figure 12: This ternary diagram shows that the feldspar inclusions in our Bo Rai samples fall within the plagioclase range (bytownite and andesine).

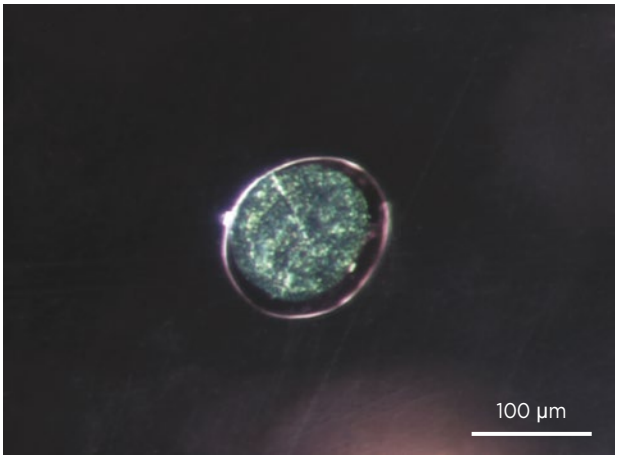

Figure 14: The sulphide inclusions in Bo Rai rubies typically form rounded to sub-hexagonal opaque grains that appear black, although they may show metallic reflections (causing the greenish grey appearance seen here). Photomicrograph by S. Promwongnan; darkfield illumination with fibre-optic light.

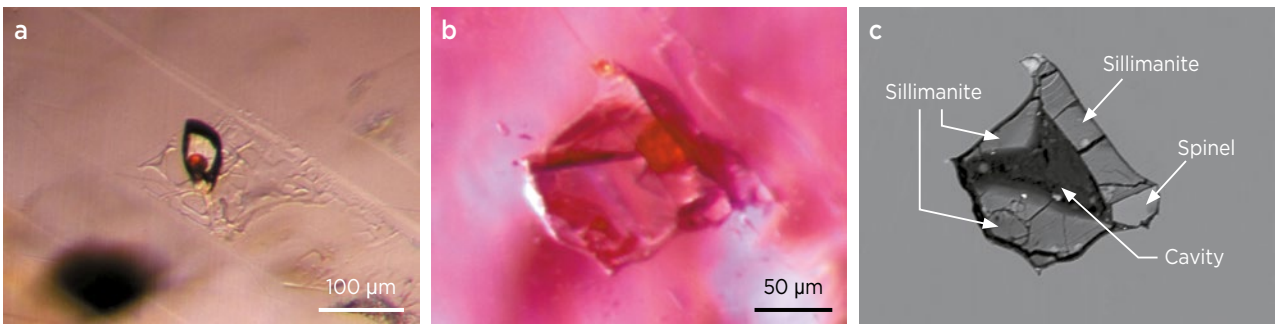

Figure 13: (**a**) The colourless crystal seen here in a Bo Rai ruby, identified as sillimanite, is hosted by a fluid inclusion and itself contains a rounded area of red material. (**b**) Sillimanite also forms part of a subhedral composite inclusion along with spinel. (**c**) The sillimanite and spinel components of the composite inclusion are clearly visible with the use of backscattered-electron imaging. Photomicrographs by S. Promwongnan; brightfield illumination with fibre-optic light (a, b).

Table V: Representative EPMA analyses of sulphide inclusions in the Bo Rai ruby sample set.

Sample no.	9TRA214-1	9TRA160-1	9TRA176-1	9TRA208-1	9TRA055-1	9TRA231-1	9TRA202-1
Element (wt.%)							
Al	0.09	0.04	0.06	0.05	0.04	0.11	0.03
S	18.71	19.35	14.93	22.12	27.72	25.34	26.49
Ti	0.29	nd*	0.04	0.21	0.37	0.18	0.3
Fe	9.39	9.19	9.21	21.61	34.68	42.42	31.21
Ni	0.06	0.06	4.59	0.14	22.63	4.58	11.67
Co	nd	na*	nd	nd	na	na	nd
Cu	62.17	64.39	51.69	42.88	0.03	1.05	18.32
Zn	nd	na	nd	nd	na	na	nd
As	nd	na	nd	nd	na	na	nd
Mo	0.23	0.39	0.43	0.44	0.42	0.44	0.45
In	0.01	nd	nd	0.05	nd	nd	nd
Sn	nd	na	nd	nd	na	na	nd
Ba	0.28	0.35	0.27	0.22	nd	nd	0.11
Pt	nd	nd	nd	nd	0.02	0.14	0.04
Pb	nd	nd	nd	nd	nd	nd	nd
Total	91.24	93.78	81.22	87.71	85.90	74.25	88.63

*Abbreviations: na = not analysed, nd = not detected.

DISCUSSION

The etched patterns on the surfaces of some samples of Bo Rai ruby were apparently caused by chemical resorption in the magma. Such features are also typically observed on corundum from basaltic terranes elsewhere (Coenraads 1992).

Spectroscopic features within the mid-IR range showed the presence of a kaolinite-group mineral in these untreated rubies, which has been documented previously in basaltic-related corundum (e.g. in sapphires from southern Vietnam: Smith *et al.* 1995). This hydrous phase appears to form in corundum as a secondary product (Smith *et al.* 1995; Beran & Rossman 2006; Schwarz *et al.* 2008) and may be used as an indicator of an unheated stone.

UV-Vis-NIR spectra of the rP to P samples commonly showed iron- and chromium-related absorption features, consistent with their chemical compositions, in particular an Fe_2O_3:Cr_2O_3 ratio that was usually >3.

The most common mineral inclusion observed in our samples from Bo Rai was Al-rich pyroxene, which had compositions similar to those of pyroxenes associated with alluvial rubies from Bo Rai and Pailin (Sutherland *et al.* 1998b; Sutthirat *et al.* 2001), as well as those found in ruby-bearing mafic granulite xenoliths in alkali basalt from Bo Rai (Sutthirat *et al.* 2018). The pyroxene inclusions analysed in this study were also similar to ruby-bearing mafic xenocrysts embedded in alkali basalt from the Nong Bon gem field (Sutthirat *et al.* 2001), located about 20 km west of Bo Rai.

The Cr-poor pyrope inclusions in Bo Rai ruby have compositions that are similar to those of garnet xenocrysts embedded in Nong Bon basalt and to garnet in mafic xenoliths from Bo Welu (located ~30 km northwest of Bo Rai), which were documented by Sutthirat *et al.* (2001) and Saminpanya & Sutherland (2011), respectively. Plagioclase was reported previously as an inclusion in Thai ruby by Gübelin (1971), although the compositions of such inclusions were not documented until now. The spinel inclusions analysed in this study contained greater Mg than that of a pleonastic spinel inclusion found in ruby from western Pailin in Cambodia (Sutherland *et al.* 1998b). The varying composition of the sulphide inclusions in Bo Rai rubies may reflect locally heterogeneous formational environments. Gübelin (1971) documented chalcopyrite ($CuFeS_2$) in Thai rubies, and additional sulphide minerals have been reported by other researchers.

Overall, the inclusion assemblage in Bo Rai ruby—particularly clinopyroxene, garnet, plagioclase and spinel—closely resembles the minerals composing ruby-bearing mafic granulite xenoliths (plagioclase + clinopyroxene + spinel ± garnet ± corundum) in basalts surrounding the Bo Rai gem field (Promprated *et al.* 2003; Sutthirat *et al.* 2018). The mineral chemistries of these assemblages are also comparable, indicating that the alluvial rubies originally crystallised in mafic granulites prior to being transported to the surface via basaltic eruptions. Weathering of the basalts resulted in the accumulation of gem corundum within the alluvial

deposits. Based on the isotope study of Yui *et al.* (2006), mafic metamorphic rock was suggested to be related to the original formation of Thai ruby. This agrees with corundum formation in mafic granulites, which are high-grade metamorphic rocks.

Palke *et al.* (2018) documented melt inclusions in reddish violet sapphire from Yogo Gulch, Montana, USA, and in rubies from Thailand and Cambodia, with similar compositions of 53.4–60.5% SiO_2, 20.6–24.0% Al_2O_3, 4.9–6.2% CaO and 4.3–5.2% Na_2O with negligible Ti, Mg, Fe and K. These melt compositions were interpreted together with trace elements and oxygen isotopic analyses of their corundum hosts. In their genetic model, Palke *et al.* (2018) suggested that Thai ruby was associated with the transformation of anorthosite to garnet pyroxenite along with a partial melting process. The melt inclusions found in our Bo Rai ruby samples contained approximately 48.5–56.5% SiO_2, 26.4–31.9% Al_2O_3, 9.7–11.1% CaO, 1.6–2.0% FeO_{tot}, 3.0–3.2% MgO and 0.8–1.4% Na_2O, and therefore have lower Si and Na contents and higher Al, Ca, Fe and Mg contents compared to those reported by Palke *et al.* (2018). These variations in composition could relate to different degrees of partial melting and crystallisation. The presence of sillimanite and silicate melt inclusions in the Bo Rai samples clearly suggests exposure to high temperatures (>500ºC), consistent with partial melting, prior to the crystallisation of Thai ruby.

CONCLUSIONS

Bo Rai rubies commonly contain minute mineral inclusions surrounded by equatorial thin films. In addition, various mineral inclusions were identified in this study, particularly pyroxene, pyrope and plagioclase and minor spinel, which is consistent with the inferred original source rock of mafic granulite. Moreover, sillimanite and silicate melt inclusions indicate a high-temperature environment during crystallisation. The presence of sillimanite and spinel inclusions is described here for the first time in Thai ruby.

REFERENCES

Beran, A. & Rossman, G.R. 2006. OH in naturally occurring corundum. *European Journal of Mineralogy*, **18**(4), 441–447, http://doi.org/10.1127/0935-1221/2006/0018-0441.

Clark, J.R. & Papike, J. 1968. Crystal-chemical characterization of omphacites. *American Mineralogist*, **53**(5–6), 840–868.

Coenraads, R.R. 1992. Surface features on natural rubies and sapphires derived from volcanic provinces. *Journal of Gemmology*, **23**(3), 151–160, http://doi.org/10.15506/JoG.1992.23.3.151.

Droop, G.T.R. 1987. A general equation for estimating Fe^{3+} concentrations in ferromagnesian silicates and oxides from microprobe analyses, using stoichiometric criteria. *Mineralogical Magazine*, **51**(361), 431–435, http://doi.org/10.1180/minmag.1987.051.361.10.

Gübelin, E. 1940. Differences between Burma and Siam rubies. *Gems & Gemology*, **3**(5), 69–72.

Gübelin, E. 1971. New analytical results of the inclusions in Siam rubies. *Journal of Gemmology*, **12**(7), 242–252, http://doi.org/10.15506/JoG.1971.12.7.242.

Gübelin, E.J. & Koivula, J.I. 1986. *Photoatlas of Inclusions in Gemstones*. ABC Edition, Zurich, Switzerland, 532 pp.

Guo, J., Griffin, W.L. & O'Reilly, S.Y. 1994. A cobalt-rich spinel inclusion in a sapphire from Bo Ploi, Thailand. *Mineralogical Magazine*, **58**(391), 247–258, http://doi.org/10.1180/minmag.1994.058.391.07.

Hughes, R.W. 2017. *Ruby & Sapphire: A Gemologist's Guide*. RWH Publishing, Bangkok, Thailand, 816 pp.

Intasopa, S., Atichat, W., Pisutha-Arnond, V., Sriprasert, B., Narudeesombat, N. & Puttharat, T. 1999. Inclusions in Chanthaburi-Trat corundums: A clue to their genesis. *Symposium on Mineral, Energy and Water Resources of Thailand: Towards the Year 2000*, Bangkok, Thailand, 28–29 October, 471–484 (in Thai).

Keller, P.C. 1982. The Chanthaburi-Trat gem field, Thailand. *Gems & Gemology*, **18**(2), 186–196, https://doi.org/10.5741/gems.18.4.186.

Khamloet, P., Pisutha-Arnond, V. & Sutthirat, C. 2014. Mineral inclusions in sapphire from the basalt-related deposit in Bo Phloi, Kanchanaburi, western Thailand: Indication of their genesis. *Russian Geology and Geophysics*, **55**(9), 1087–1102, http://doi.org/10.1016/j.rgg.2014.08.004.

Koivula, J.I. & Fryer, C.W. 1987. Sapphirine (not sapphire) in a ruby from Bo Rai, Thailand. *Journal of Gemmology*, **20**(6), 369–370, http://doi.org/10.15506/JoG.1987.20.6.369.

Morimoto, N., Fabries, J., Ferguson, A.K., Ginzburg, I.V., Ross, M., Seifert, F.A., Zussman, J., Aoki, K. & Gottardi, G. 1988. Nomenclature of pyroxenes. *American Mineralogist*, **73**(9–10), 1123–1133.

Palke, A.C., Wong, J., Verdel, C. & Ávila, J.N. 2018. A common origin for Thai/Cambodian rubies and blue and violet sapphires from Yogo Gulch, Montana, U.S.A.? *American Mineralogist*, **103**(3), 469–479, http://doi.org/10.2138/am-2018-6164.

Pattamalai, K., 2015. Chanthaburi-Trat corundum deposits, eastern Thailand. *Proceedings of the 3rd Lao-Thai Technical Conference on Geology and Mineral Resources*, Bangkok, Thailand, 7–11 July, 219–229.

Promprated, P., Taylor, L.A. & Neal, C.R. 2003. Petrochemistry of mafic granulite xenoliths from the Chantaburi [*sic*] basaltic field: Implications for the nature of the lower crust beneath Thailand. *International Geology Review*, **45**(5), 383–406, http://doi.org/10.2747/0020-6814.45.5.383.

Saeseaw, S., Sangsawong, S., Vertriest, W., Atikarnsakul, U., Raynaud-Flattot, V.L., Khowpong, C. & Weeramonkhonlert, V. 2017. *A Study of Sapphire from Chanthaburi, Thailand and Its Gemological Characteristics.* Gemological Institute of America, 12 April, 42 pp., www.gia.edu/doc/Blue-sapphires-Chantaburi-Thailand-finalfinal.pdf.

Saminpanya, S. & Sutherland, F.L. 2011. Different origins of Thai area sapphire and ruby, derived from mineral inclusions and co-existing minerals. *European Journal of Mineralogy*, **23**(4), 683–694, http://doi.org/10.1127/0935-1221/2011/0023-2123.

Saminpanya, S., Manning, D.A.C., Droop, G.T.R. & Henderson, C.M.B. 2003. Trace elements in Thai gem corundums. *Journal of Gemmology*, **28**(7), 399–416, http://doi.org/10.15506/JoG.2003.28.7.399.

Sangsawong, S., Vertriest, W., Saeseaw, S., Pardieu, V., Muyal, J., Khowpong, C., Atikarnsakul, U. & Weeramonkhonlert, V. 2017. *A Study of Rubies from Cambodia and Thailand*. Gemological Institute of America, July, 37 pp., www.gia.edu/gia-news-research/study-rubies-cambodia-thailand.

Schwarz, D., Pardieu, V., Saul, J.M., Schmetzer, K., Laurs, B.M., Giuliani, G., Klemm, L., Malsy, A.-K., Erel, E., Hauzenberger, C., Du Toit, G., Fallick, A.E. & Ohnenstetter, D. 2008. Rubies and sapphires from Winza, central Tanzania. *Gems & Gemology*, **44**(4), 322–347, http://doi.org/10.5741/gems.44.4.322.

Smith, C.P., Kammerling, R.C., Keller, A.S., Peretti, A., Scarratt, K.V., Khoa, N.D. & Repetto, S. 1995. Sapphires from southern Vietnam. *Gems & Gemology*, **31**(3), 168–186, http://doi.org/10.5741/gems.31.3.168.

Sutherland, F.L., Hoskin, P.W.O., Fanning, C.M. & Coenraads, R.R. 1998a. Models of corundum origin from alkali basaltic terrains: A reappraisal. *Contributions to Mineralogy and Petrology*, **133**(4), 356–372, http://doi.org/10.1007/s004100050458.

Sutherland, F.L., Schwarz, D., Jobbins, E.A., Coenraads, R.R. & Webb, G. 1998b. Distinctive gem corundum suites from discrete basalt fields: A comparative study of Barrington, Australia, and West Pailin, Cambodia, gemfields. *Journal of Gemmology*, **26**(2), 65–85, http://doi.org/10.15506/JoG.1998.26.2.65.

Sutthirat, C., Charusiri, P., Farrar, E. & Clark, A.H. 1994. New $^{40}Ar/^{39}Ar$ geochronology and characteristics of some Cenozoic basalts in Thailand. *Proceedings of the International Symposium on Stratigraphic Correlation of Southeast Asia, 15–20 November 1994, Bangkok, Thailand*. Department of Mineral Resources and IGCP 306, Bangkok, Thailand, 306–321.

Sutthirat, C., Saminpanya, S., Droop, G.T.R., Henderson, C.M.B. & Manning, D.A.C. 2001. Clinopyroxene-corundum assemblages from alkali basalt and alluvium, eastern Thailand: Constraints on the origin of Thai rubies. *Mineralogical Magazine*, **65**(2), 277–295, http://doi.org/10.1180/002646101550253.

Sutthirat, C., Hauzenberger, C., Chualaowanich, T. & Assawincharoenkij, T. 2018. Mantle and deep crustal xenoliths in basalts from the Bo Rai ruby deposit, eastern Thailand: Original source of basaltic ruby. *Journal of Asian Earth Sciences*, **164**, 366–379, http://doi.org/10.1016/j.jseaes.2018.07.006.

Vichit, P. 1992. Gemstones in Thailand. *In*: Piencharoen, C. (ed) *Proceedings of a National Conference on Geologic Resources of Thailand—Potential for Future Development: 17–24 November 1992, Bangkok, Thailand*. Department of Mineral Resources, Bangkok, Thailand, 124–150.

Vichit, P., Vudhichativanich, S. & Hansawek, R. 1978. The distribution and some characteristics of corundum-bearing basalts in Thailand. *Journal of the Geological Society of Thailand*, **3**, M4-1–M4-38.

Yui, T.-F., Wu, C.-M., Limtrakun, P., Sricharn, W. & Boonsoong, A. 2006. Oxygen isotope studies on placer sapphire and ruby in the Chanthaburi-Trat alkali basaltic gemfield, Thailand. *Lithos*, **86**(3–4), 197–211, http://doi.org/10.1016/j.lithos.2005.06.002.

The Authors

Supparat Promwongnan
Geology Department, Faculty of Science, Chulalongkorn University, Bangkok, Thailand, and Gem Testing Laboratory, Gem and Jewelry Institute of Thailand (GIT), Bangkok, Thailand
Email: psupparat@git.or.th

Dr Chakkaphan Sutthirat
Faculty of Science and Environmental Research Institute, Chulalongkorn University, Bangkok, Thailand
Email: chakkaphan.s@chula.ac.th

Acknowledgements

The authors thank Thai Lapidary International Co. Ltd and Prima Gems (Bangkok, Thailand), as well as an anonymous private collector, for loaning stones and jewellery for photography. This research was supported financially by the 90th Anniversary of Chulalongkorn University, Rachadapisek Sompote Fund of Chulalongkorn University. The first author would like to thank Duangkamol Jiambutr (GIT director), Wilawan Atichat, Dr Visut Pisutha-Arnond, Thanong Leelawatanasuk and Dr Sakonvan Chawchai for their suggestions and encouragement throughout her M.Sc. studies. Special thanks also go to Sopit Poompeang for assistance with sample preparation and EPMA analyses.